Iranian Journal of Chemical Engineering

Journal Homepage: www.ijche.com

pISSN: 1735-5397
eISSN: 2008-2355

Regular Article

CFD Modeling of the Dehydration of Biofuels with the 2D MXene Membrane using the Pervaporation Process

N. Hajilary [1*], S. Hashemi [1], M. Hajiabadi [2]

[1] Department of Chemical Engineering, Faculty of Engineering, Golestan University, Aliabad Katoul, Iran
[2] Department of Mechanical Engineering, Faculty of Engineering, Khaje Nasir Toosi University, Tehran, Iran

ARTICLE INFO

Article history:
Received: 2022-05-30
Accepted: 2022-08-22
Available online: 2022-08-22

Keywords:
Biofuel,
Dehydration,
Pervaporation,
MXene,
CFD

ABSTRACT

MXene membranes perform well in biofuel separation due to their excellent hydrophilicity, flexibility, and mechanical strength. For the first time, computational fluid dynamics was used to model the dehydration of ethanol through the pervaporation system by the MXene membrane. We discretized the momentum and continuity equations using finite element methods and predicted the mass transport. Experimental results and model data were in good agreement (less than 10 %). The feed velocity, feed concentration, and membrane thickness all had positive effects on the separation factors while the temperature had a decreasing effect. This model's efficiency has decreased by 35 % after increasing the feed flow rate by 10 times. In addition, the separation factor increases tenfold when temperature is raised from 25 to 70 °C.

DOI: 10.22034/ijche.2022.344611.1440 URL: http://www.ijche.com/article_155093.html

1. Introduction

As human societies developed, and consequently the consumption of primary resources increased, the use of secondary resources and enhancing the efficiency of exploitation of these resources became more important. Sorting and separation processes in factories are used for the analysis, upgrading, and concentration of secondary resources that are compatible with the environment, preventing the release of pollutants and impurities. These processes are also efficient in terms of energy, equipment, and natural resources [1].

Separation methods include distillation, adsorption, crystallization, liquid-liquid extraction, and membrane separation. The membrane separation method, despite its short history compared to other methods, has been attractive in the last two decades due to its simplicity, low energy consumption, cost-effectiveness, and high efficiency.

*Corresponding author: n.hajilari@gu.ac.ir (N. Hajilari)

Pervaporation is one of the membrane separation methods, which is mostly used to separate liquid mixtures through the partial vaporization with a porous or non-porous membrane. It is more cost-effective than the evaporation process mechanism, which relies on the difference in boiling points [2].

Pervaporation is an efficient way to separate organic compounds, especially aromatics, in industries such as the chemical, food, and pharmaceutical industries. In the past, ethanol was used only in a few industries as an organic substance, but it is now considered one of the most valuable and strategically important commodities in many countries. Therefore, in this project, the pervaporation process was used to purify ethanol. Membrane separations with pervaporation have a wide range of applications, including the dehydration, desalination, and separation of organic mixtures. It can be used for systems containing azeotropes that cannot be separated using traditional distillation methods [3].

For the first time, Wu, et al. used 2 -thick MXene membranes ($Ti_3C_2T_x$ nanoparticles) for the water/ethanol separation. Using the pervaporation process, the water/ethanol separation factor with the MXene membrane increased as the concentration of feed ethanol increased. According to them, the MXene membrane performs better at room temperature than at high temperatures. At room temperature, a separation factor of 135.2 is obtained for 95 % of ethanol mixed with 5 % of water, with a flux of 263.4 $gm^{-2}h^{-1}$. A major advantage of MXene membranes is their higher permeability when soaked in solvents, increasing the water/ethanol separation factor, and providing an alternative to the traditional distillation for the ethanol dehydration process [4].

In 2019, Wu and his colleagues studied the morphology, chemical structure, and hydrophilicity of membrane membranes by SEM, AFM, IR, XPS, and water contact angle measurements. Three types of organic solvents, ethanol, ethyl acetate, and dimethyl carbonate were used to evaluate the membrane efficiency performance. The results showed that the composition of MXene nano-sheets did not increase the surface adsorption, while MXene sheets assembled with interlayer channels greatly increased the molecular penetration of water through the membrane. Therefore, the flux of the chitosan (CS) membrane separation agent was improved simultaneously with the introduction of MXene nanosheets. Optimized MXene\CS displays an overall flux of 1.4 to 1.5 kg/(m^2.h) and a separation factor of 1421, 4898 and 906 for the dehydration of ethanol, ethyl acetate and dimethyl carbonate at 50 °C respectively. This performance is higher than those of advanced membranes, and therefore indicates the high ability of MXene- based membranes to separate water in the biofuel solutions [5].

Due to the thickness of the membrane, Zhou and his colleagues were able to improve the purification efficiency by using two-dimensional kaolin nanosheets. Among the membranes tested, MXene composites have hgh conductivity and diversity. MXenes are two-dimensional ceramic plates made of carbides, nitrides, and conductive metals such as titanium and molybdenum [6].

In a study conducted by Liu and his colleagues in 2016 and 2018, 60 nm MXene $Ti_3C_2T_x$ thin-film plates were used for the desalination by pervaporation, during which at 65 °C the separation efficiency was 99.5 % [7]. In another study , MXene $Ti_3C_2T_x$ thin-film plates separated 95 % of the particles

smaller than 2.5 nm [8].

In 2018, Srimuk used a $Mo_{1.33}C$-MXene molybdenum membrane to separate more than 95 % of salt from water. In 2017, Han and his colleagues examined the significant increase in the hydrophilicity and flux capability of MXene composite membranes [9].

The ZIF-71\PDMS nanocomposite is applied to recover ethanol and 1- butanol from water. They prepared different solutions of zeolite with the concentration values of 0, 5, 25, and 40 % by weight to evaluate the performance of the separation method. They found that by increasing the amount of zeolite (40 % by weight), the highest amount of the separation and selectivity of ethanol and 1-butanol from water occurred [10].

In another study, a PDMS composite membrane coated on nanocarbons was used to separate the acetone-butanol-ethanol organic mixture by pervaporation. It is observed that by increasing the amount of nanocarbons, the separation factor increased [11].

For the pervaporation desalination, thin membranes with the thickness of a few tens of nanometers were developed by stacking the atomic-thin nanosheets of MXene. As effective parameters on the membrane performance, the lateral size of MXene nanosheets and the feed temperature have been studied. When used in artificial seawater systems, the membrane showed good salt removal, high water flux, and long-term stability [8].

To model and analyze the fluid flow of pervaporation systems, the computational fluid dynamics (CFD) is a strong tool. With the CFD simulation of the PV process, system drawbacks are removed and membranes with high efficiency are designed. The operational conditions also can be optimized and the process is improved. In addition, with the employed CFD analysis, the cost and time consumed for PV experiments decreased significantly [12]. A hollow fiber membrane with several baffles and bundles of NaA zeolite membranes was modeled using CFD. With two radial baffles and four axial baffles, it shows uniform flow distribution inside the membrane module [13]. The research by Hadddi et al. introduces a new CFD algorithm. For fast process simulation applications, one dimension is used, whereas three dimensions are used for fully resolved CFD applications. Based on experiments performed on a hollow fiber module, 1 and 3 dimensional simulations were compared fairly well with less than 2 % deviation of globale scale. In 3D simulations, high velocity zones can be observed close to the module walls because of the arrangement of fibers. A pilot-scale biogas separation module was simulated in co- and counter-current configurations, demonstrating that the one dimension CFD works well even for almost pure gasses [14]. In 2019, Quiroz-perez and his colleagues, in a review study on the use of the computational fluid dynamics in modeling and the refinement of the core equipment for liquid biofuel production processes, especially considered the following biofuels; Bioethanol, biodiesel and green diesel. In addition, they provided an analysis of the progress and challenges in this area. They found that most of research efforts focused on biodiesel production processes, along with some studies on green diesel, bioethanol, and biobutanol. In addition, they mentioned that modeling chemical reactions in CFD studies which focused on bioalcohol production technologies did not attract sufficient attention. By increasing computational resources, problems with low computational

memory in current CFD models, such as the limited representation of the actual size of the computational range, refined meshes, multi-physical models (flow, turbulence, energy and mass transfer, and chemical reactions) can be overcome. Thus, the use of CFD for producing biofuel at industrail scale is a key area of opportunity for research and development [15].

The performance of the pervaporation technique is modeled to purify water in a polyvinyl alcohol membrane unit using the finite element method, which uses computational dynamics to solve the model equations. The model was validated using experimental data; the simulation results were consistent with the experimental data of different values of the feed flow rate and temperature. Also, the finding of the model indicates that the infiltration flux increases by increasing the flow rate and temperature per membrane unit [16].

In the purification of cyclohexane with PDMS membranes, the effect of the concentration of the feed on the separation factor was studied. The separation factor for a mixture containing 80 wt % of cyclohexane and a temperature of 300 K was 2500 at a vacuum pressure of 100 mmHg. Also, a two-dimensional mechanical model was proposed to predict the amount of the cyclohexane mass transfer from the membrane and the concentration distribution during the process. Based on the effect of the distribution of the mass transfer rate, it was found that the highest cyclohexane transfer flux occurs near the inlet of the supply channel, while the flux at the top of the module is zero [17].

There have been numerous reports about MXene-based membranes in recent years. These membranes have demonstrated remarkable performance in terms of permeance and selectivity. In order to overcome the empirical trade-off barrier, it is vitally important to model how MXene-based membranes achieve these incredible performance levels. However, there has never been a report on modeling pristine MXene membranes used for the dehydration of ethanol.

Despite many efforts to fabricate different membranes to increase the separation efficiency and reduce the costs of the process, the need for the selective membrane fabrication in the pervaporation process as well as the optimization of process conditions such as temperature, pressure, and concentration still exists. MXene membranes should still be improved compared to other permeable membranes in the water/ethanol separation process. Thus, the performance of the MXene nanocomposite as a new two-dimensional membrane in the pervaporation process is simulated in order to increase the controllability of the separation process and achieve a suitable membrane. In the simulation, the Comsol software known as COMSOL Multiphysics was used.

2. Experimental

The MXene membrane was prepared by the vacuum filtration of the diluted $Ti_3C_2T_x$ nanosheets solution on a Nylon microfiltration membrane. The MXene membrane with a typical wave-like structure and 2 μm thickness was used for the removal of water from the ethanol/water mixture by the pervaporation setup. The detailed procedure of synthesizing the membrane and the dehydration of ethanol were explained elsewhere [5]. Feed solutions containing the ethanol/water liquid mixture with different percentages of water in different temperatures were applied.

3. Mathematical modeling

A schematic diagram of the model domain is presented in Figure 1. A liquid mixture consisting of 90 wt % of ethanol and 10 wt % of water as a feed passes through the upper side of the model in x=o. Ethanol as a permeate diffuses through the MXene membrane in the y direction due to the differential chemical potential that is represented as a concentration gradient between the phase on the opposite side of the membrane. The membrane at y=H is ended.

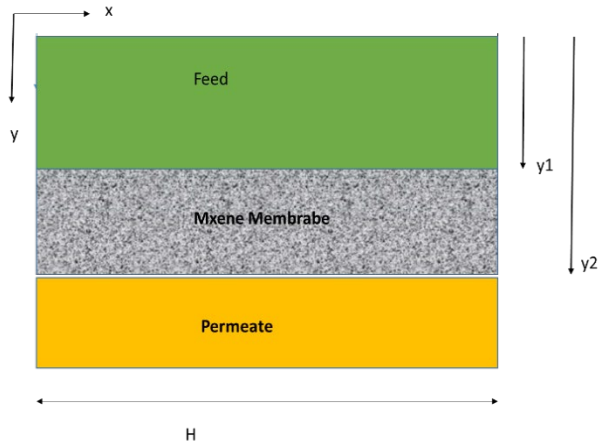

Figure 1. Model domain and relevant boundaries.

The transport of materials through the membrane in pervaporation can be described by a solution desorption model based on different molecular sizes of the feed component. It supposes: 1) components diffuse through the liquid side to the membrane, 2) sorption/diffusion through the membrane, 3) transport across the membrane, 4) diffusion through the vapor side into the permeate bulk.

The assumptions considered in this mathematical modeling were as follows:

1) At the vapor phase the resistance made by the boundary layer is negligible.

2) At the permeate side the concentration of the solute is zero.

3) The system is in isothermal conditions and steady state.

4) The feed in the membrane module is laminar.

5) The thermodynamic equilibrium exists at the interface of the feed and the membrane.

6) The mass transfer resistance of the support layer is negligible.

The mass transfer of water from the feed side to the permeate bulk is described by a continuity equation. The main equation of the mass transfer called diffusion and convection equation, which obtained from mass balance of water, is written in the differential form as:

$$\frac{\partial C_W}{\partial t} + \nabla.(-D_W \nabla C_W + C_W V) = R_W \qquad (1)$$

where C_W, D_W, V, t and R_W represent the concentration of water (mol/m^3), diffusion coefficient (m^2/s), velocity (m/s), time (s) and reaction term respectively. The velocity distribution can be driven from momentum equations or be expressed analytically. The concentration distribution of water is obtained from solving equation (1) numerically. To solve the quantity equation, the distribution of velocity vectors is required. So the Navier-Stokes equation as a momentum equation should be coupled with a continuity equation and solved simultaneously. The Navier stoke equation for laminar flow is as follows:

$$-\nabla \cdot \eta(\nabla V_y + (\nabla V_y)^{\tau}) + \rho(V_y \cdot \nabla)V_y + \nabla P = F \qquad (2)$$

$$\nabla \cdot V_y = 0 \qquad (3)$$

where η represents the dynamic viscosity (kg/m.s), V_Y is velocity vector in y-direction (m/s), ρ is the density of the fluid (kg/m^3), P is pressure (Pa), and F is the body force term. X-velocity should be solved since the feed flow is in the x-direction.

The boundary condition for Navier-Stokes is as follows:

x=0, $v_y=v_0$ (inlet velocity)

x=H, v=0 (no slip conditions)

y=0 $p=p_{atm}$

y=a v=0 (no slip conditions)

The next step is to solve the mass transfer equation. In the membrane module, the component distribution is obtained by simultaneously solving the coupled quantity and momentum equations.

3.1. Feed side

The water transport into the boundary layer on the liquid feed phase is given by Ficks law of diffusion to estimate the diffusive flux:

$$D_w\left(\left(\frac{\partial^2 C_{w\_f}}{\partial x^2}\right)+\frac{\partial^2 C_{w\_f}}{\partial y^2}\right)=V_x\frac{\partial C_{w\_f}}{\partial x} \quad (4)$$

where D_w denotes the diffusion coefficient (m^2/s), $C_{w\text{-}f}$ denotes the concentration of water (mol/m^2), and v is the velocity vector in the x-direction (m/s). Velocity in the x-direction should be solved due to the feed flow in the y direction. In a convective flux boundary condition, convection dominates all mass passing through the boundary. The initial assumption is that there will be no mass flux across the boundary due to diffusion. The boundary conditions for this equation are:

at x = 0 $C_{wf}= C_0$ (inlet concentration)

at x = H $\frac{\partial C_{w\_f}}{\partial x}=0$ (insulation boundary)

at y = 0 convective flux

at x = 0 $c_{wf}= c_{wf/m}$

where c_0 and m are the concentration of the inlet and water partition coefficient between the feed and membrane. The convective flux in the boundary condition assumes all the mass across this boundary is passed by convection and the mass transfer by diffusion is negligible.

3.2. Membrane side

The continuity equation for the water transport across the membrane in a steady state is given by:

$$D_{w-m}\left(\left(\frac{\partial^2 C_{w-m}}{\partial x^2}\right)+\frac{\partial^2 C_{w-m}}{\partial y^2}\right)=0 \quad (5)$$

The boundary condition of the continuity equation on the side is as follows:

at x = 0 and x = H $\frac{\partial C_{w-m}}{\partial x}=0$ (insulation boundary)

at y = a $c_{wm}=c_{wf}\times m$

at y=b $c_{wm}=0$

It is necessary to say at y = b vacuum happens.

3.3. Heat transfer equation

The distribution of temperature in the membrane module is obtained by the general heat transfer equation. Equation (6) considers both methods of heat transfer including convection and conduction.

$$\rho C_P\frac{\partial T}{\partial t}+\nabla\cdot(-k\nabla T)=Q+q_s T-\rho C_P u\cdot\nabla T \quad (6)$$

C_p, k, T, u, q_s and Q denote the heat capacity at constant pressure $\left({}^{J}/_{Kg\,K}\right)$, the thermal conductivity $\left({}^{W}/_{m\,K}\right)$, temperature (k), velocity (m/s), the production/absorption coefficient (W/m^3K) and the heat source. This paper calculates the permeability flux (J) using the following equation:

$$J=\frac{M}{A.t} \quad (7)$$

where M (kg) represents the total mass transferred, t (hr) is the operation time , and A (m^2) is the effective area of the membrane. According to equation (8), the separation

factor (α_{ij}) can be calculated as:

$$\alpha_{ij} = \frac{y_{wi}/y_{wj}}{x_{wi}/x_{wj}} \quad (8)$$

The performance of the membrane is measured by the separation factor (α_{ij}) defined in equation 8 where y_w and x_w are the weight fractions of the components in the penetration and feed sides respectively. The indicators i and j relate to the two separating components of the feed mixture solution.

4. Results and discussion

4.1. Validation

The effect of the composition of the feed on the membrane performance in the dehydration of ethanol with different concentrations of 75 to 95 % by weight of ethanol as the feed solution at room temperature are presented in Figure 2. The gradient trend of the graph changes uniformly with the experimental data, and the graph has the same trend as the experimental data. The experimental and model data are thus well matched.

4.2. Water distribution

Figure 2 shows that the separation factor of the mixture of ethanol and water increases as the ethanol content of the feed increases.

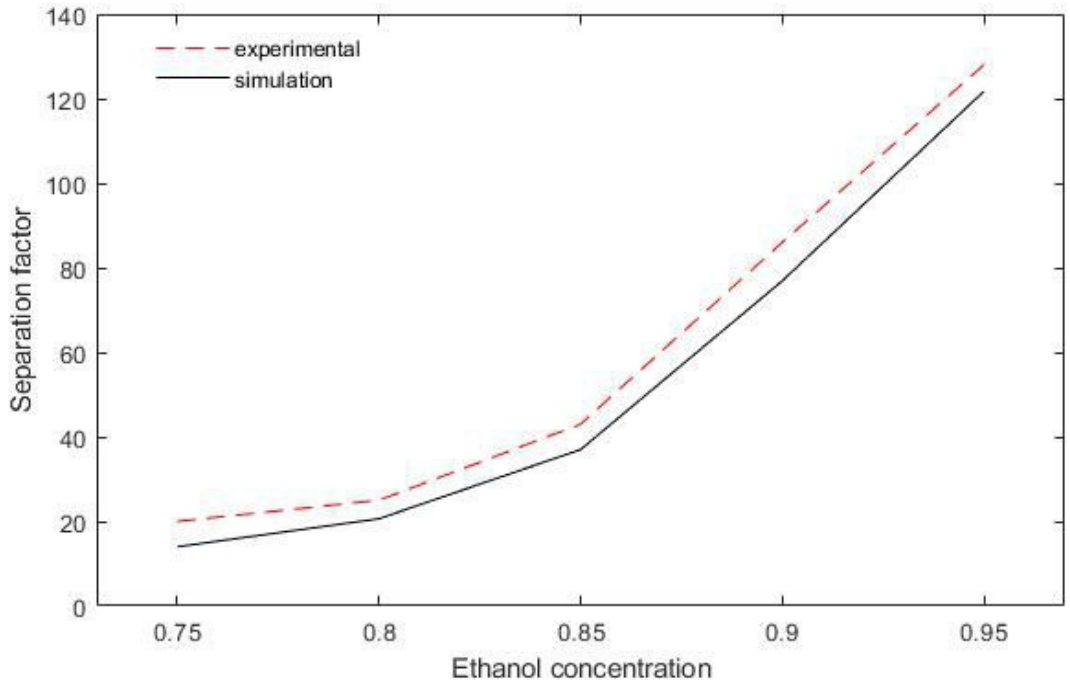

Figure 2. Comparing the simulation and experimental value for the effect of the composition of the feed on the membrane performance in the dehydration of ethanol at room temperature.

The concentrations between 75 and 85 % result in the separation factors below 50 %. To be effective, the concentration of ethanol must be above 85 %. As the concentration increased, the separation factor increased with a steep slope.

Although the incorporation of MXene nanosheets did not improve the surface sorption, MXene laminates with interlayer channels greatly enhanced the permeation of water molecules through the membrane.

Figure 3 shows the dimensionless distribution of water in various parts of the MXene membrane module. An ethanol-water mixture flows from the feed side, where the concentration of ethanol is highest. A

chemical potential difference, or concentration difference, enables water to pass through the membrane. The mass transport in the feed side of the module is explained by convection and diffusion. Water passes through the membrane using a diffusion mechanism, reaches the saturation pressure and evaporates by maintaining a vacuum on the permeate side. We assume that there is no concentration of water at the interface between the permeate and membrane because of the low pressure.

There are three measuring tapes in Figure 3; the upper one corresponds to the feed inlet part, the middle one to the membrane, and the lower one to the product. The concentration of water decreases as it gets closer to the membrane's end, indicating that separation has taken place. Another study confirmed these results [16]. Regarding this figure, it is also worth mentioning that the separation is done well around 2 cm and then the concentration gradient is negligible. Since it is difficult to make different types of membranes and ensure the proper performance, instead of increasing the length of the membrane, the solution is circulated several times.

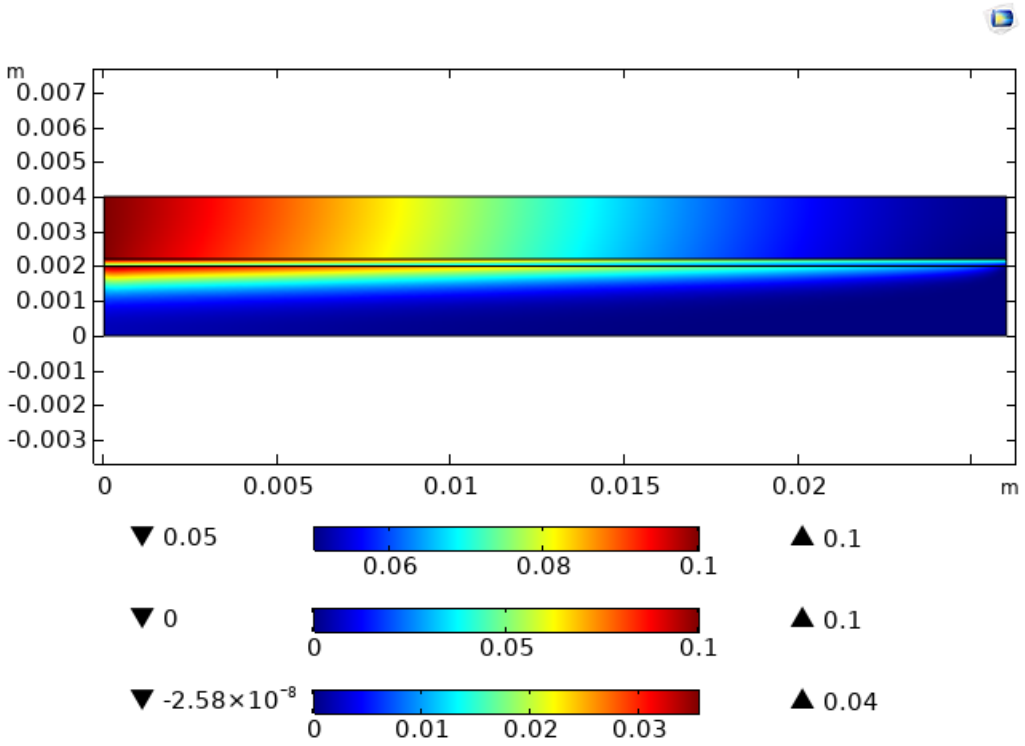

Figure 3. Distribution of the concentration of water in the MXene membrane of the module.

4.3. Temperature of the PV process

As shown in Table 1, the water/ethanol separation factor is a function of the temperature performance. In the pervaporation process, the feed temperature affects both the diffusion and solubility of the species in the membrane. The feed temperatures were set at 25, 40, 50, 60, and 70 °C in experimentation and simulation. Based on the results, the separation factor increases by increasing the process temperature at the concentration of 90 wt % of the ethanol feed. An explanation for this can be found in the solution-diffusion mechanism. With a higher pressure on the feed side than the same on the permeate side,

components pass through a membrane. The vapor pressure gradient across the membrane for the component transport increased by increasing the feed temperature. As a result of a greater difference in the saturation pressure at a higher temperature, the diving force increases and the permeation flux increases. In addition, the thermal motion of polymer chains can produce the random free volume in amorphous regions, and molecules can diffuse through the free volume of the membrane. By increasing the temperature, polymer-jumping chains multiply in number and amplitude, increasing the membrane's free volume. Therefore, the permeation component diffuses more rapidly, resulting in a higher separation factor. Increasing the feed temperature could also accelerate the phase transitions of the permeates inside the membrane, since the enthalpy of the transition is rapidly reached when more heat is supplied. Therefore, diffusion and mass transfer are faster across the membrane.

In Table 1, the errors of the simulation and experimental results are below 10 %, which indicates that the model estimations are well matched to the experimental results.

Table 1
Data obtained from the effect of the temperature applied on the membrane performance in the dehydration of the feed containing 90 % of ethanol.

Test temperature (°C)	Separation factor		Error (%)
	Experimental data	Model data	
25	87	87.9	1.02
40	82	83.47	1.76
50	76	78.52	3.21
60	58	63.26	8.31
70	38	42.23	10.02

4.4. Velocity distribution

In the membrane module, the velocity distribution was modeled using Navier-Stokes equations. It increases the accuracy of the estimation model by taking into account entry effects (Figure 4). The top bar shows the velocity distribution in the feed side and the bottom bar shows the velocity distribution in the membrane side. In the product area, the velocity is almost maximum due to the suction conditions, but in the feed section, the velocity is lower. In the feed side, feed enters the module via the forced displacement, but in the separated side, only concentration differences drive the movement.

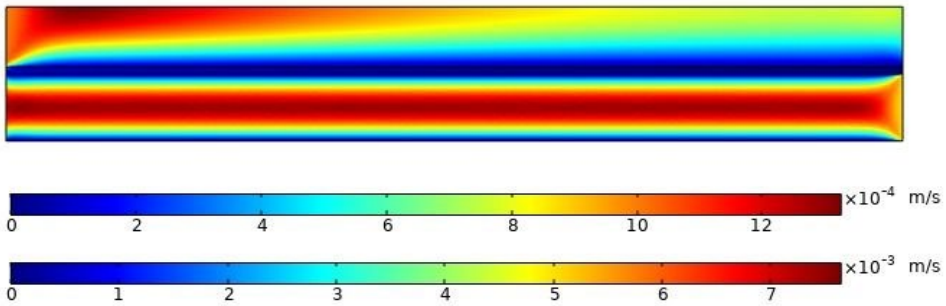

Figure 4. Distribution of velocity in different parts of the MXene membrane module.

Figure 5 shows the axial velocity profile via the length of the module for the feed section. This curve clearly shows that there is a maximum velocity near the entrance of the module. Additionally, as it moves towards the membrane's end, its velocity decreases.

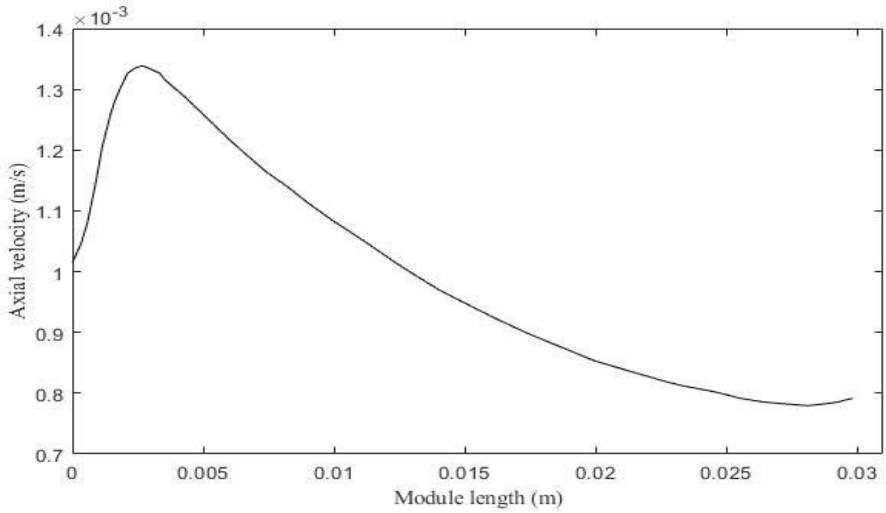

Figure 5. Distribution of the axial velocity along the modules feed side.

4.5. Feed flow rate

Figure 6 illustrates the effect of the feed flow rate on the separation efficiency. As the feed flow rate increases, the separation factor decreases. The concentration polarization can explain these results [18]. During the pervaporation process, the liquid boundary layer on the feed side is stagnant, and as the feed flow rate increases, the resistance of the boundary layer reduces, thus the mass transport is enhanced. By increasing the speed by 10 times, this model's efficiency has decreased by 35 %.

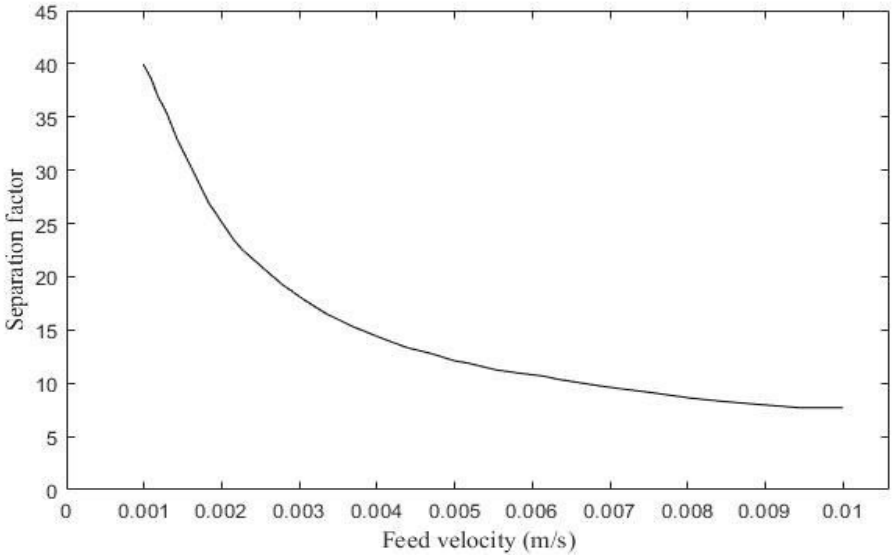

Figure 6. The separation factor in terms of the feed velocity.

4.6. Membrane thickness

Figure 7 shows the effect of the membrane thickness on the separation factor. Separation factors increase by increasing the membrane

thickness. By increasing the membrane thickness, mass transfer pathways become longer and the flux decreases. If it is reduced too much, the mechanical strength may be decreased, which may reduce the efficiency.

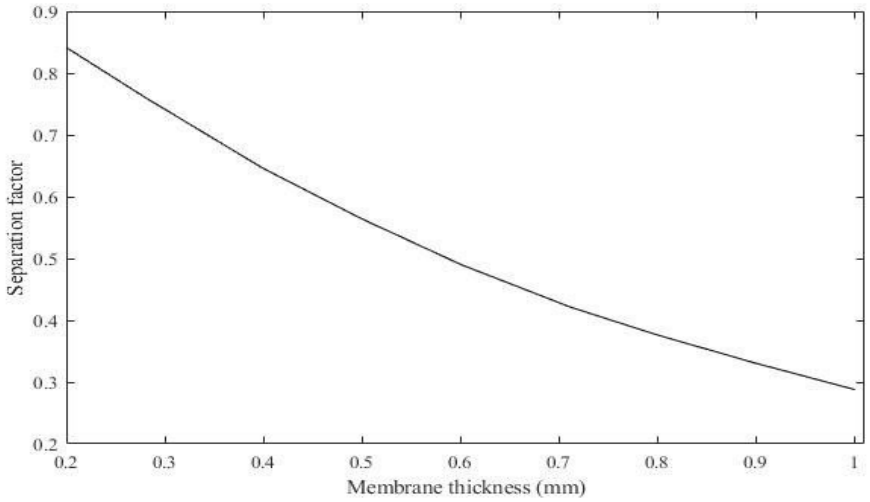

Figure 7. Separation factor via the membrane thickness.

5. Conclusions

We studied the separation of water from the ethanol/water mixture using MXene membranes. We developed a two-dimensional mathematical model to predict the flow of water through a membrane during pervaporation. Using the model, the continuity, heat, and mass transfer equations for the components are solved numerically. The validation of the model was carried out using the experimental data from a MXene membrane in a PV experiment. The comparison between the experimental and simulated results for different concentrations of the permeate showed good agreement. The effects of the concentration, velocity, temperature, model length, and membrane thickness of the feed on the permeate flux of composites were examined. After increasing the feed flow rate by ten times, this model's efficiency decreased by 35 % and the concentrations of ethanol must be above 85 % in order to be effective. A ten time increase in the separation factor is observed when the temperature is raised from 25 to 70 °C.

Acknowledgement

The authors gratefully acknowledge the financial support of Golestan university, Gorgan, Iran, No. 1496.

Nomenclature

2D	2 dimensional.
E_D	activation energy of diffusion [J/mol].
CFD	Computational Fluid Dynamics.
C	concentration [mol/m^3].
r	density of the fuid [kg/m^3].
D	diffusion coefficient [m^2/s].
h	dynamic viscosity [kg/m s].
A	effective membrane surface area [m^2].
FEM	Finite Element Method.
C_p	heat capacity [J/kg K].
Q	heat source [W/ m^3].
MSE	Molecular Surface Engineering.
M	permeate weight [kg].
J_p	permeation flux [kg/m^2h].
PV	Pervaporation.
T	pervaporation time [h].
P	pressure [Pa].
q_s	production/absorption coefficient [W/m^3k].
T	temperature [k].
TBA	Tery-Butyl Alcohol.

k	thermal conductivity [W/m k].
δ	time- scaling coefficient.
J	total flux [kg/m^2 h].
u	velocity of the fluid [m/s].
V	velocity vector [m/s].
x	X coordinate [m].
y	Y coordinate [m].
xi(x_i^F)	permeable component weight fraction in feed.
x_j	non-permeable component weight fraction in feed.
y_i(y_i^p)	permeable component weight fraction in permeate.
y_j	non-permeable component weight fraction in permeate.
F	body force term [N].

Superscripts and subscripts

w	water.
y	y-direction.
m	membrane.
i	interface.

References

[1] Baker, R. W., Membrane technology and applications, 2nd ed., John Wiley & sons publication, California, USA, p. 124 (2004).

[2] Srikanth, G., "Membrane separation processes: Technology and business opportunities", *Chem. Eng. World*, **34** (5), 55 (1999).

[3] Luis, P., Fundamental modelling of membrane systems: Membrane and process performance, 1st ed. EUROMEMBRANE, (2018). (http://hdl.handle.net/2078.1/241732).

[4] Wu, Y., Ding, L., Lu, Z., Deng, J. and Wei, Y., "Two-dimensional MXene membrane for ethanol dehydration", *J. Memb. Sci.*, **590** (1), 1 (2019). (https://doi.org/10.1016/j.memsci.2019.117300).

[5] Xu, Z., Liu, G., Ye, H., Jin, W. and Cui, Z., "Two-dimensional MXene incorporated chitosan mixed-matrix membranes for efficient solvent dehydration", *J. Memb. Sci.*, **563** (1), 625 (2018). (https://doi.org/10.1016/j.memsci.2018.05.044).

[6] Liu, T., Zhou, H., Graham, N., Yu, W. and Sun, K., "2D kaolin ultrafiltration membrane with ultrahigh flux for water purification", *Water Res.*, **156**, 425 (2019). (https://doi.org/10.1016/j.watres.2019.03.050).

[7] Liu, G., Hung, W. S., Shen, J., Li, Q., Huang, Y. H., Jin, W.,Lee, K. R. and Lai, J. Y., "Mixed matrix membranes with molecular-interaction-driven tunable free volumes for efficient bio-fuel recovery", *J. Mater. Chem. A*, **3** (8), 4510, (2015). (https://doi.org/10.1039/c4ta05881j).

[8] Liu, G., Shen, J., Liu, Q., Xiong, G., Yang, J. and Jin, W., "Ultrathin two-dimensional MXene membrane for pervaporation desalination"," *J. Memb. Sci.*, **548**, 548 (2018). (https://doi.org/10.1016/j.memsci.2017.11.065).

[9] Srimuk, P., Halim, J., Lee, J., Tao, Q., Rosen, J. and Presser, V., "Two-dimensional molybdenum carbide (MXene) with divacancy ordering for brackish and seawater desalination via cation and anion intercalation", *ACS Sustain. Chem. Eng.*, **6** (3), 3739 (2018). (https://doi.org/10.1021/acssuschemeng.7b04095).

[10] Naik, P. V., Kerkhofs, S., Martens, J. A. and Vankelecom, I. F. J., "PDMS mixed matrix membranes containing hollow silicalite sphere for ethanol / water separation by pervaporation", *J. Memb. Sci.*, **502**, 48 (2016). (https://doi.org/10.1016/j.memsci.2015.12.028).

[11] Azimi, H., Ebneyamini, A., Tezel, F. H. and Thibault, J., "Separation of organic compounds from ABE model solutions via pervaporation using activated carbon/PDMS mixed matrix membranes", *Membranes (Basel).*, **8** (3), 1 (2018). (https://doi.org/10.3390/membranes8030040).

[12] Aryafard, E., Rahmatmand, B. and Rahimpour, M. R., "Application of computational fluid dynamics technique in pervaporation processes", In Current Trends and Future Developments on (Bio-) Membranes, 247 (2022). (https://doi.org/10.1016/B978-0-12-822294-2.00012-6).

[13] Wang, J., Gao, X., Ji, G. and Gu, X., "CFD simulation of hollow fiber supported NaA zeolite membrane modules", *Separation and Purification Technology,* **213**, 1 (2019). (https://doi.org/org/10.1016/j.seppur.2018.12.017).

[14] Haddadi, B., Jordan, C., Miltner, M. and Harasek, M., "Membrane modeling using CFD: Combined evaluation of mass transfer and geometrical influences in 1D and 3D", *Journal of Membrane Science,* **563**, 199 (2018). (https://doi.org/10.1016/j.memsci.2018.05.040).

[15] Quiroz-Pérez, E., Gutiérrez-Antonio, C. and Vázquez-Román, R., "Modelling of production processes for liquid biofuels through CFD: A review of conventional and intensified technologies", *Chem. Eng. Process. - Process Intensif.*, **143** (2), 107629 (2019). (https://doi.org/10.1016/j.cep.2019.107629).

[16] Rezakazemi, M., Shahverdi, M., Shirazian, S., Mohammadi, T. and Pak, A., "CFD simulation of water removal from water/ethylene glycol mixtures by pervaporation", *Chem. Eng. J.*, **168** (1), 60 (2011). (https://doi.org/10.1016/j.cej.2010.12.034).

[17] Rezakazemi, M., Marjani, A. and Shirazian, S., "Organic solvent removal by pervaporation membrane technology: Experimental and simulation", *Environ. Sci. Pollut. Res.*, **25** (20), 19818 (2018). (https://doi.org/10.1007/s11356-018-2155-3).

[18] She, M. and Hwag, S. T., "Conentration of dilute flavor compounds by pervaporation: Permeate effect and boundary layer resistance modeling", *J. Member. Sci.*, **236**, 193 (2004).